Elsevier Editorial System(tm) for Applied Thermal Engineering

Manuscript Draft

Manuscript Number:

Title: Effect of extreme wetting scenarios on pool boiling conditions in a quiescent medium

Article Type: SI:UKHTC 2015

Keywords: Pool Boiling; Superhydrophobicity; Wettability; Boiling onset; Boiling Curve; Bubble dynamics

Corresponding Author: Dr. Ana Moita, PhD

Corresponding Author's Institution: Instituto Superior Técnico - TU Lisbon

First Author: Emanuele Teodori, Master

Order of Authors: Emanuele Teodori, Master; Tomas Valente, Master; Ileana Malavasi, Master; Ana Moita, PhD; Marco Marengo, PhD; António L Moreira, PhD

Abstract: This study focuses on the detailed description of the heat transfer and bubble dynamics processes occurring for the boiling of water on surfaces with extreme wetting regimes, namely hydrophilicity and superhydrophobicity. The wettability is changed at the expense of modifying the surface chemistry and without significant variations in the mean surface roughness. Under these conditions and for the range studied here the effect of the extreme wetting regimes was dominant, thus the influence of surface topography was not addressed. A particular trend is observed for the boiling curve obtained with the superhydrophobic surfaces, as the heat flux increases almost linearly with the superheat, although with a much lower slope than the hydrophilic surfaces. This occurs due to the formation of a large stable vapour film over the entire surface just at around 1K superheat, as a result of the almost immediate coalescence of the bubbles generated on the surface. This behaviour is in agreement with the so-called "quasi-Leidenfrost" regime recently reported in the literature and with a theoretical prediction of the heat flux that is presented in the present study; furthermore here a comprehensive analysis of bubble dynamics, useful for comparison with numerical simulations is given. Such analysis is based on the temporal evolution of the bubble diameter together with bubble contact angle and with the velocity of the contact line. The results suggest that the existing models and correlations can predict the trends of the bubble growth using a modified contact angle value, called the bubble contact angle (or its supplemental value), for the hydrophilic surfaces, even if they cannot accurately predict bubble sizes. Approximating the modified contact angle with the quasi-static contact angle, obtained during surface characterization, is practical for a qualitative evaluation, but the results obtained here do not support for its use when estimating the bubble departure diameter. On superhydrophobic surfaces, the effect of the vapour film must be considered, since although this is not the starting point of the boiling process, it represents the actual working conditions when using this kind of surfaces.

Effect of extreme wetting scenarios on pool boiling conditions in a quiescent medium

E. Teodori[a], T. Valente[a], I. Malavasi[b], A.S. Moita[*a], M. Marengo[b,c], A.L.N. Moreira[a]

[a]IN+ - Instituto Superior Técnico, Universidade de Lisboa, Av. Rovisco Pais, 1049-001 Lisbon, Portugal
[b]Dept. of Eng. and Applied Sciences, University of Bergamo, Viale Marconi 5, 24044 Dalmine, Italy
[c]University of Brighton, School of Computing, Engineering and Mathematics, Lewes Road, BN2 4GJ Brighton, UK

Corresponding author:

A.S. Moita (anamoita@dem.ist.utl.pt)

Phone: +351-21 841 7876

Fax: +351-21 849 6156

Address: IN+ - Center for Innovation, Technology and Policy Research, Instituto Superior Técnico, Universidade de Lisboa, Av. Rovisco Pais, 1049-001 Lisboa, Portugal.

KEYWORDS

Pool Boiling, Superhydrophobicity, Wettability, Boiling onset, Boiling Curve, Bubble dynamics

HIGHLIGHTS

- Detailed pool boiling bubble dynamics on extreme wetting regimes is performed
- Under extreme wetting regimes, wettability plays a dominant role
- "Quasi-Leidenfrost" regime is supported by comparison with theoretical predictions
- The macro-contact angle can be used in correlations predicting bubble size
- Apparent angles should not be approximated to quasi-static values for predictions

ABSTRACT

This study focuses on the detailed description of the heat transfer and bubble dynamics processes occurring for the boiling of water on surfaces with extreme wetting regimes, namely hydrophilicity and superhydrophobicity. The wettability is changed at the expense of modifying the surface chemistry and without significant variations in the mean surface roughness. Under these conditions and for the range studied here the effect of the extreme wetting regimes was dominant, thus the influence of surface topography was not addressed. A particular trend is observed for the boiling curve obtained with the superhydrophobic surfaces, as the heat flux increases almost linearly with the superheat, although with a much lower slope than the hydrophilic surfaces. This occurs due to the formation of a large stable vapour film over the entire surface just at around 1K superheat, as a result of the almost immediate coalescence of the bubbles generated on the surface. This behaviour is in agreement with the so-called "quasi-Leidenfrost" regime recently reported in the literature and with a theoretical prediction of the heat flux that is presented in the present study; furthermore here a comprehensive analysis of bubble dynamics, useful for comparison with numerical simulations is given. Such analysis is based on the temporal evolution of the bubble diameter together with bubble contact angle and with the velocity of the contact line. The results suggest that the existing models and correlations can predict the trends of the bubble growth using a modified contact angle value, called the bubble contact angle (or its supplemental value), for the hydrophilic surfaces, even if they cannot accurately predict bubble sizes. Approximating the modified contact angle with the quasi-static contact angle, obtained during surface characterization, is practical for a qualitative evaluation, but the results obtained here do not support for its use when estimating the bubble departure diameter. On superhydrophobic surfaces, the effect of the vapour film must be considered, since although this is not the starting point of the boiling process, it represents the actual working conditions when using this kind of surfaces.

Nomenclature

Latin letters

q''	(W/cm^2)	Heat flux
D_b	(mm)	Bubble departure diameter
C_p	(J/kgK)	Specific heat
f_b	(Hz)	Bubble emission frequency
g	(m/s^2)	Gravity acceleration constant
h	($W/(m^2K)$)	Heat transfer coefficient
h_{fg}	(kJ/kg)	Latent heat of evaporation
K	(W/(mK))	Thermal conductivity
L_c	(mm)	Characteristic length (capillary length)
R_a	(µm)	Surface mean roughness
R_z	(µm)	Surface peak-to-valley roughness
T	(^oC)	Temperature

Greek symbols

α	(m^2/s)	Thermal diffusivity
µ	(Ns/m^2)	Dynamic viscosity
θ_{adv}	(^{o})	Quasi-static advancing contact angle
θ_{rec}	(^{o})	Quasi-static receding contact angle

θ_e	(^{o})	Apparent equilibrium contact angle
θ_μ	(^{o})	Micro contact angle
ρ	(kg/m^3)	Density
σ	(N/m)	Interfacial tension

Subscripts

B	Bubble
e	Equilibrium
L	Liquid
V	Vapor

1. Introduction

Enhancement of pool boiling heat transfer is often achieved by altering surface properties. The evolution observed in micro-and-nano-fabrication techniques within the last decade provides the researchers the opportunity to test a wide range of surface treatments, which quickly evolved from the micro-patterned surfaces [1] to nano-coatings [2,3]. Nonetheless, many of these treatments simultaneously alter surface topography and wettability in a non-systematic way, turning difficult to understand dominant effects on the boiling mechanisms. In fact the wettability is affected by the chemistry of the surface (and of the working fluid) and by the surface topography. However, it is possible and desirable to separate them at some extent, as recently shown by Bourdon et al. [4,5]. The surface wettability is usually roughly quantified by the apparent equilibrium contact angle θ_e, which is obtained at the equilibrium between the interfacial tensions acting at liquid-solid-vapor contact interfaces (often measured on a sessile drop deposited on the surface). Based on this apparent angle, it is widely accepted that a surface is lyophilic (i.e. promotes the liquid spreading) for $0<\theta_e<90^o$ and lyophobic (i.e. repels the liquid) for $\theta_e>90^o$. The terms hydrophilic/hydrophobic, which are commonly used for liquid attractive/repellent surfaces, derive from the specific attraction/repellence of water. The boundaries for extreme wetting scenarios, namely superhydrophilicity and superhydrophobicity are still debated in the most recent literature, as universal criteria to determine stable extreme wetting regimes are not easily defined. It is known that the heterogeneous wetting regime associated to superhydrophobicity may not be stable and may not hold, as an activation energy barrier is transposed and the contact line slowly moves [6]. Hence, the most representative measures are given by the quasi-static advancing or receding contact angles and by the hysteresis, which is basically the difference between the quasi-static advancing and the receding angles. So, based on this, several authors, such as Bhushan and Jung [7], consider that a surface is superhydrophobic for $\theta_{adv}>150^o$, as long as the hysteresis is lower than 10^o. These advancing and receding angles are also argued to be more representative of dynamic processes, as demonstrated for drop impacts (for example in [8]). For bubbles however, the vapour is over the surface and surrounded by the liquid, so the balance of the interfacial forces is different, as illustrated in Fig. 1.

Addressing the effect of wettability in bubble generation and detachment, quantified by a contact angle is a complex task that has been debated for many years. Several authors consider a rough approximation of the equilibrium angle to be representative of the wettability effect on the contact angle at bubble formation and growth. For instance, considering homogeneous nucleation, pioneering theories, such as that proposed by Bankoff [9] establish an energy factor which mainly represents the ratio of the energy required to form a bubble with the apparent equilibrium contact angle θ_e on the surface and the energy required to form a full sphere with the same diameter. This factor is maximum at θ_e=0º (complete wetting) and minimum at θ_e=180º (non-wetting system). Even though Bankoff's theory for homogeneous nucleation, considers that bubble growth is mainly due to evaporation of the superheated liquid layer that surrounds the bubble after inception (e.g. [10,11]), similar arguments have been recently used by Phan et al [3] and by Cheng et al. [12] for heterogeneous nucleation, considering that the bubble growth is grounded on the evaporation from the base of the bubble, where a microlayer between the liquid-vapour interface and the solid surface is formed. Considering the variation of the free Gibbs energy (or of the so-called availability function, as proposed by Cheng et al. [12]) these authors

show that bubble nucleation starts at lower superheat values on a superhydrophobic surface, as the energy barrier necessary for nucleus generation is smaller.

Figure 1

Given that the critical conditions for boiling incipience are taken for static equilibrium, the use of static parameters seems adequate for the initial growth behaviour [13]. However, the definition of the adequate contact angle during bubble growth until detachment is not so clear. For instance, [3] establish general trends between the size of the bubbles (at detachment) and the static contact angle. However, when predicting the bubble detachment diameter, Phan et al. [3] report an opposite trend of the bubble growth with the static contact angle, when compared to that given by the Fritz's equation [14]. The accuracy of Fritz's equation has further been debated several times, particularly when dealing with hydrophobic and superhydrophobic surfaces [15]. Hence, as an alternative approach, Phan et al. [3] define a micro-contact angle, θ_μ between the micro-layer and the liquid-vapour interface. Evaporation at this region leads to a distortion in the mechanical equilibrium and therefore the contact line changes its shape from Fig. 2a) to Fig 2b) [16]. Consequently, a micro and a macro contact angles can be identified (Fig. 2b). For a hydrophilic surface, the contact line moves during bubble growth until this micro-angle reaches 90º (Fig. 2c) and starts then to recede towards the bubble axis (Fig. 2d) until bubble detachment (Fig 2e). However, this θ_μ is impractical to measure, so Phan et al. [3-17] further explain the bubble growth process, based on the macro-angle. Recognizing the importance of hysteresis and the use of quasi-static advancing and receding angles for the bubble growth scenario as previously reported for instance by [18], Phan et al [3] argue that as the convex vapour appears at the cavity shape, the contact angle is the equilibrium angle (at saturated temperature), which is kept when the bubble forms at the cavity mouth. As the liquid microlayer evaporates at the base of the bubble, the bubble grows and the macro-angle is approximated to the quasi-static receding angle. The force balance further leads the contact line to recede and the macro-contact angle approaches the quasi-static advancing angle. On the other hand, for lyophobic surfaces, the presence of the microlayer is not so clear, so that only the macro-contact angle is defined (Fig 2f). The macro-angle is still approximated to the equilibrium angle as a concave vapour shape appears and later the bubble forms at the cavity mouth. The contact angle also approaches the receding angle during bubble growth, but then, since there is no interfacial tension component to push the bubble or contribute to its detachment from the surface, the bubble radius keeps increasing with a macro-angle close to the advancing angle.

Figure 2

The global description of the aforementioned processes allows a qualitative explanation that is in agreement with the main trends consistently reported in the various experiments performed on pool boiling over superhydrophobic vs hydrophilic surfaces (e.g. [2,3,19,20]: the onset of boiling occurs at very low superheat values on superhydrophobic surfaces, but then as the force balance does not favour the bubble release, large bubbles stay for longer attached on the surface and coalesce, leading to a Critical Heat Flux condition at low superheat values. Conversely, a hydrophilic surface requires larger superheat to start bubble nucleation, but find it easier to release the vapour bubble, so that higher CHF can be reached.

However, in this kind of descriptions, the contact angles are continuously being re-defined and approximated to account for the effect on wettability on bubble growth. On the other hand, a detailed description of the nucleation process and of bubble dynamics such as those performed for instance by Phan et al [3], McHale and Garimella [21] and Moita et al. [22] are still scarce and do not allow establishing the accurate relation between bubble dynamics and the aforementioned trends of the boiling curves. An accurate and practical quantity that can satisfactorily account for the wettability on the bubble formation is therefore important to understand the related heat transfer mechanisms, as the main heat transfer processes are currently known to occur during bubble growth and detachment [23-25]. Within this scope, the present work aims at contributing with additional information to allow a more adequate description of bubble dynamics and discusses on the adequate parameters relating these dynamic processes with surface wettability. Hence, boiling curves obtained for extreme wetting scenarios (hydrophilic vs superhydrophobic) are described in detail and related to the corresponding bubble dynamics, characterized by the temporal evolution of several quantities, namely bubble diameter, bubble emission frequency, bubble contact angle and contact line motion. The quantification of these variables is supporting further numerical simulations of the boiling process. Moreover, the surface topography is varied within these extreme wetting conditions, in a systematic and controlled way to assess on its role in a situation for which the wettability is mainly controlled by the chemical modification of the surface.

2. Experimental analysis

2.1. Experimental set-up

The set-up is mainly composed by a boiling chamber, a degassing system of the working fluid, pressurized and constantly heated and filling and evacuating circuits, which connect the boiling chamber respectively to the degassing station and to the waste fluid container, being the latter at ambient pressure. The boiling chamber, which is schematically represented in Fig. 3 has approximately a cubic shape with 200mm side. Heaters disposed inside and on the outer walls of the boiling chamber are controlled by a PID controller to assure that the liquid remains inside the chamber at saturation temperature. The boiling chamber is isolated from the outside with thermal resistant natural rubber. The type K thermocouple which acquires the data to characterize the saturation state of the liquid is located 25mm above the test surface. The temperature and the pressure inside the boiling chamber are accurately controlled with a precision of 1^{o}C and 1.6 mbar, respectively.

The pressure is controlled by means of two electronic valves, which are actuated based on the measures given by a pressure transducer (OMEGA DYNE Inc.) inside the chamber, using a home-made software based loop control. This control system allows the pressure

variations to be lower than 5mbar. The refilling and the entire measurement processes are automatically controlled by this routine. The temperatures are sampled using type K and type T thermocouples. The signal is acquired and amplified by a National Instruments DAQ board connected with a BNC2120.

The heating block, which heats and accommodates the different surfaces, comprises a copper cylinder, with a dimeter of 20mm, inside which a cartridge heater (up to 315W) is placed. The cylinder is isolated with Teflon, from the outside. The surfaces are positioned into the heating block using a custom made system with bolts and springs, to assure reproducible thermal contact. The bolts contacting the surface are made from PEEK (polyether ether ketone) to minimize the heat that is dissipated from the surface to the bolts. The heat flux is measured using a thin heat flux meter (Captec Entreprise®) custom made to fit perfectly to the heating block. This heat flux meter, which is placed between the copper cylinder and the surface, has a sensitivity of 2.21 mV/(W/m^2). The surface temperature is measured with a T-type thermocouple that is coupled with the heat flux meter. The accuracy of this thermocouple is ±0.5K.

Figure 3

2.2. Experimental procedures

The test surfaces are characterized in terms of their superficial topography and wettability, before and after each essay (corresponding to a single boiling curve), as detailed in the following paragraphs. This procedure ensures the exact definition of the boundary conditions related to the wettability and allows inferring the effect of surface ageing on the wettability and, consequently on the pool boiling curves. Then, pool boiling curves are constructed for each test surface, which are obtained by slowly imposing the heat flux in small increasing power steps. For each power step increased, bubble dynamics and nucleation mechanisms are also characterized based on visualization, using a high-speed camera (Phantom v4.2 from Vision Research Inc.). Quantitative information regarding bubble dynamics is further obtained by image post-processing procedures. The working fluid is degassed distilled water. The thermo-physical properties relevant to this study are summarized in **Error! Reference source not found.**.

Table 1

The pool boiling tests start by degassing the distilled water for about 30min being the degassing procedure kept during the entire test. Before filling the boiling chamber, a vacuum pump is used to remove air from the chamber. This pump stays on throughout the entire filling process until the chamber is completely full to minimize the possibility of keeping air entrapped that would be dissolved in the working fluid, which would affect the saturation temperature. The fluid is degassed by applying full power to the internal resistances until the saturation temperature is achieved for the measured pressure, thus assuring that the fluid is degassed within the uncertainty of the measurement instruments.

2.2.1 Surface preparation

Stainless steel surfaces are prepared to have dissimilar topographic and wetting properties. The numerous surfaces used in this study (nearly 40) are divided in 4 main categories (see Table 2): RAW – "smooth" hydrophilic surfaces, ROUGH – "rough" hydrophilic surfaces, RAW SHS and ROUGH SHS, representing superhydrophobic surfaces with identical roughness amplitude as that of the hydrophilic ones. The superhydrophobic surfaces are obtained at the expense of a chemical coating (a commercial compound called Glaco Mirror Coat Zero, from Soft99 Co, which is mainly a perfluoroalkyltrichlorosilane combined with perfluoropolyether carboxylic acid and a fluorinated solvent [26]). All the surfaces are first cleaned, following the main steps: a) 30 min in an ultrasonic bath in water at 40^{o}C, b) drying with compressed air and c) 30 min in an ultrasonic bath in acetone at 40^{o}C. Then the coating is applied as in [27]. The aforementioned cleaning procedure must be repeated for each surface and for all the boiling curves.

2.2.2 Characterization of the surfaces

The homogeneity of surface topography and morphology is checked by Laser Scanning Confocal Microscopy (Leica SP8 Confocal Microscope) using the reflection mode. Then, the stochastic roughness profiles are measured using a Dektak 3 profile meter (Veeco) with a vertical resolution of 20nm. These profiles are further processed to obtain the mean roughness (determined according to standard BS1134) and the mean peak-to-valley roughness (determined following standard DIN4768). Average representative values of R_a and R_z are taken from 10 measurements distributed along the entire surface.

Wettability is quantified by the apparent quasi-static advancing and receding angles. Hysteresis (i.e. the difference between the quasi-static advancing and receding angles) is also evaluated for the coated surfaces to assure that it was lower than 10^{o} for the superhydrophobic surfaces (following the criterion presented in the Introduction). The measurements are performed at room temperature (20^{o}C±3ºC), using an optical tensiometer (TETA from Attention). The angles are evaluated from the images taken within the tensiometer, using a camera adapted to a microscope. The images (with resolution of 15.6 µm/pixel for the optical configuration used) are post-processed by a drop detection algorithm based on the Young-Laplace equation (One Attention software). The accuracy of these algorithms is argued to be of the order of ± 0.1^{o} [28]. Overall, the manufacturer assures ±1^{o} for the contact angle measurement accuracy, but their uncertainty depends on the reproducibility of the measurements, which is affected by the homogeneity of the surface. Nevertheless, **Error! Reference source not found.**, which depicts the main characteristics of the four categories of surfaces defined for the present study shows that the contact angle measurements were reproducible, being the values presented here taken as an average of 3 representative measurements distributed along the surface. Deviations in R_a were admitted around 10% within each category.

Table 2

2.3. Data reduction and uncertainties

2.3.1 Pool boiling curves

The boiling curves are obtained under imposed heat flux conditions on the surface, with continuous control and monitoring of the surface temperature, liquid temperature and pressure inside the pool boiling chamber. The data is acquired under controlled pressure conditions, at 1 bar ± 10mbar for each surface and the curves constructed by varying the imposed heat flux in small steps of 1-5W until the maximum safe working temperature of the heat flux sensor is attained (180ºC). This procedure allows obtaining 10-11 points per curve in one experiment. In each point, three seconds of data for heat flux and pressure are recorded at 100 Hz and for every one hundred data points, its average and standard deviations are written to a spreadsheet. Simultaneously, one thousand points of surface and fluid temperature are recorded and the average and standard deviation values are calculated. Each final curve is averaged from 4 experiments. Since the temperature provided by the heat flux sensor is that of the under part of the test surface, the boiling curves must be corrected considering the thermal resistance between heat flux sensor and the top of the surface following, which is evaluated using an high-speed infrared thermographic camera - ONCA-MWIR-InSb-320 infrared camera from Xenics (ONCA 4696 series). To reduce errors due to emissivity the surface was painted in black (ε= 0.95-0.96).

The uncertainty in the temperature measurements ΔT is assessed according to [29]:

$$\Delta T = \sqrt{U^2 + (2S)^2} \quad (1)$$

U is the uncertainty of the measurement instrument itself, which in this case is $\pm 0.5^{o}$ for the thermocouple embedded in the heat flux sensor, and S is the standard deviation of the measurements. Following this, the maximum uncertainty for the temperature measurements is ±0.95K.

On the other hand, the error associated with heat flux measurement in the sensor can be evaluated as:

$$\Delta q'' = \sqrt{U^2 + (2S)^2} \quad (2)$$

In this case, the uncertainty value, given by the manufacturer, is of ±3% and the maximum uncertainty in the heat flux measurements is 3.3%.

2.3.2 Bubble dynamics

The characterization of the nucleation mechanisms and bubble dynamics is based on high-speed visualization and image post-processing. Images of 512/512pixel^2 are recorded with a frame rate of 2200fps and a spatial resolution of 31.85µm/pixel. A home-made routine developed in MATLAB enables determining the temporal evolution of the bubble diameter (until detachment), bubble contact angle, velocity of the contact line and bubble departure frequency. The temporal evolution of bubble growth is measured for each test condition, from the entire bubble growth period until detachment. Then, averaged (bubble diameter) values are taken, for the instant of bubble detachment for various detachment events. The bubble departure frequency is estimated by counting the number of detachment events in a defined time interval. Table 3 depicts the maximum uncertainty of the

aforementioned quantities, evaluated according to the expressions listed in the third column. For the worst case scenario, the absolute error in the contact angle measurement is estimated to be ±11.3°. This evaluation takes into account the uncertainty associated to the identification of the boundary of the bubble, which in turn affects the definition of the tangent line used to evaluate the angle.

Table 3

Results and discussion

3.1. Boiling curves

Changing the wettability within extreme scenarios leads to significant differences in the obtained boiling curves, as depicted in Fig. 4. For such extreme wetting regimes, the surface topography plays a secondary role, as its mild increase does not introduce significant changes in the boiling curves, either in the hydrophilic or in the superhydrophobic surfaces (Figs. 5). Hence a decoupled effect of surface topography and surface wettability can be achieved with the chemical surface treatment proposed. The surface topography should not play a negligible role, but for the present work, focus is put on the wettability effect.

Figure 4

Figure 5a

Figure 5b

The boiling curve obtained for the hydrophilic surfaces is quite similar to that reported in the literature (e.g. [2,3,19,20]): the onset of boiling occurs approximately for a superheating of 12K, followed by the typical increase in the curve slope, caused by the triggering of the nucleate boiling regime. It is worth mentioning that only part of the curve is represented here, still far from the Critical Heat Flux conditions.

Conversely, the boiling curve obtained for the superhydrophobic surface has an atypical tendency. The onset of boiling occurs usually during the first power step, at about 1-2K of wall superheat. Afterwards, the heat flux increases almost linearly with surface superheating, with much lower slope than that of the hydrophilic surface.

These trends can be related to bubble dynamics, as qualitatively shown in Fig. 6, which depicts the bubble generation process for various values of wall superheat, respectively for

pool boiling of water on a hydrophilic (on the left side) and superhydrophobic (on the right side) surfaces.

From the sequence of images illustrating the boiling phenomena on the hydrophilic surface, one can identify several characteristics which are often reported in the literature, for similar wetting conditions [19,20,21,30-31]: at low superheat, Fig. 6a), the nucleation sites are sparsely located within the heated area (i.e. within the diameter Φ20mm) with very few active sites. Further raising the surface superheat up to 32K, (Fig. 6c) the heated area becomes much more active with bubbles rising from a broader number of nucleation sites. Here, boiling is triggered and the slope of the boiling curve has visibly increased. Also, lateral coalescence starts to occur. This trend in increasing the number of active nucleation sites continues until the wall superheat rises typically up to 40K (Fig. 6e). Then, bubble interaction becomes chaotically evident with strong coalescence occurring in both vertical and horizontal directions. The heat flux still increases at relatively low superheat, as one is still far from the Critical Heat Flux conditions, which cannot be achieved in safe conditions for the present heat flux sensor.

On the other hand, for the superhydrophobic surfaces, even at the lowest wall superheat value, corresponding to Fig. 6b) the heated area of the superhydrophobic surface is already completely covered with a single bubble. In fact, the wall superheat value of 21K was chosen for comparative purposes, but, as aforementioned, for the superhydrophobic surface, the boiling starts immediately at 1-2K of wall superheat, although single nucleation sites are not distinguished. Instead, the boiling process is only visible by the growing of this single large bubble. Hence, further increasing the surface temperature, (Fig 6d) and f), the boiling process is not qualitatively different from that observed at lower surface superheat, except for the bubble size, since the bubble slightly grows as the wall superheat increases. Near the saturation temperature, multiple nucleation sites are in a metastable equilibrium, so that the 1-2K superheat is enough to trigger the boiling. Also, as revised in the Introduction, the energy barrier necessary for nucleus generation is smaller. Hence, very small bubbles appear on the surface already at 1-2K superheat. However, being the surface superhydrophobic, there is no interfacial tension component promoting bubble detachment, so these bubbles tend to stay attached on the surface and start to coalesce in the horizontal direction, generating an initial insulating vapor blanket from which the single bubble starts to depart, as enabled by the force balance. The particular superhydrophobicity of this surface allied to its stochastic micro-roughness, strongly promotes this behavior which occurs very fast and at very low wall superheat values, so the growth and coalescence of these small bubbles is almost impossible to capture.

This behavior is qualitatively and quantitatively in agreement with the so-called “quasi-Leidenfrost” effect recently reported by Malavasi et al. [27] to occur on surfaces similar to those used in the present study, both in the topography and in the chemical treatment. The vapor film is always stable and contrarily to the observations of [27], any intermittent rewetting is visible, even for bubble departure frequencies above 1Hz. This vapor blanket is difficult to visualize, but should be in qualitative agreement with a film boiling heat transfer trend.

Figure 6

Hence, to confirm this trend, a correlation for film boiling developed by Berenson [30], as depicted in equation (3), was compared to the experimental boiling curves obtained for the superhydrophobic surface, as shown in Fig. 7. It is worth reminding that *k* represents the thermal conductivity, ρ the density of the fluid, h_{fg} the latent heat of evaporation, C_p the specific heat, μ the dynamic viscosity, σ the liquid surface tension and *g* the gravity acceleration constant. This result must be interpreted only qualitatively, as one is using an empirical correlation, but nevertheless the qualitative interpretation shows that the relation captures a behaviour resembling the film boiling heat transfer, thus occurring over a vapour layer.

$$q'' = 0.325\left[\frac{k_v^3\rho_v g(\rho_l-\rho_v)(h_{fg}+0.4C_{pv}(T_W-T_{sat}))}{\mu_v(T_W-T_{sat})\sqrt{\sigma/g(\rho_L-\rho_v)}}\right]^{1/4}(T_W-T_{sat}) \quad (3)$$

Figure 7

The analysis performed here clearly evidence the strong relation between the boiling curves and heat transfer with bubble dynamics. In fact, the visualization of the nucleation and the bubble dynamics was particularly useful to understand the atypical trend of the boiling curves obtained for the superhydrophobic surfaces. Following this, it is now important to complement this qualitative evaluation with a detailed a quantitative analysis of the bubble dynamics, as reported in the next subsection.

3.2. Bubble dynamics

A wider overview of the trend of the average bubble departure diameter and frequency for the extreme cases of hydrophilic and superhydrophobic surfaces is depicted in Fig. 8. The results are mainly in agreement with the qualitative description of bubble dynamics discussed in the previous paragraphs.

Hence, for the hydrophilic surfaces, there is no obvious change in the average bubble size with increasing heat flux (Fig. 8a). Even though several correlations predict the increase of the bubble diameter with the heat flux for hydrophilic surfaces, others mainly address a constant departure diameter, as revised for instance in McHale and Garimella [21] and in Dhir [32]. These authors show that such trend depends on several parameters, such as the interaction mechanisms between nucleation sites. Similar observations are reported in [22]. Therefore, this result is not necessarily in disagreement with the literature. On the other hand, for the water boiling on the superhydrophobic surface, the higher heat flux increases the amount of vaporization. Considering that the large bubble is growing over the insulating vapor layer, this leads to an almost steady increase in the bubble departure diameter. Nevertheless, empirical correlations often fail to predict the bubble diameter in hydrophilic surfaces, clearly underestimating the bubble departure diameter obtained in the present work for the superhydrophobic surfaces (Fig. 8a). It is worth mentioning however that these correlations are strongly dependent from the particular experimental conditions for which they were devised. For instance the correlation of Kocamustafaogullari [31] includes high-pressure data, which does not match with the main conditions considered here. However, the large difference between the values predicted by the correlations and those obtained for the superhydrophobic surfaces is significant, thus suggesting that these relations are not addressing the physics governing the observed phenomena.

Figure 8a

Figure 8b

The difference in size of the bubble on the superhydrophobic surface, when compared to those detached from the hydrophilic surface also contributes to dissimilar results in terms of the bubble emission frequency, f_b, as depicted in Fig. 8b), being the emission frequency naturally much lower for the superhydrophobic surfaces. For the boiling on hydrophilic surfaces, on the other hand, the emission frequency follows a decreasing trend, in agreement with the behavior proposed by many correlations, including the classical relation proposed by Zuber [33]. It is worth mentioning that the bubble departure diameter and emission frequency do not have inversely proportional trends, as proposed for instance by Jakob and Fritz [34] or Mikic et al. [11], as this behavior is also strongly dependent on the interaction mechanisms, as also argued by Dhir [32] and by McHale and Garimella [21]. For the boiling on the superhydrophobic surface, the steady increase of the emission frequency is identified for increasing heat fluxes. This trend is naturally contrary to that typically reported for the hydrophilic surfaces, as expected, since the bubble formation and release process occurs over the vapor layer, so the entire growth and departure process mainly depend on the amount of vaporization.

The average values of parameters quantifying bubble dynamics, namely the departure diameter and frequency, as usually presented in the literature, are useful to identify general trends and to perform rough evaluations of the heat transfer. However, to accurately characterize the bubble growth and departure mechanisms one must not only the growth rate of the bubble, but also the motion and stability of the contact line. This detailed analysis is performed in the following paragraphs, focusing on a single nucleation.

3.2.1. Bubble dynamics (single nucleation site analysis)

Given the secondary role of the surface topography for the conditions analyzed here, the results were mainly obtained for the boiling of water over the smooth surfaces (RAW and RAW SHS, respectively for the hydrophilic and superhydrophobic scenarios).

Fig. 9 depicts the temporal evolution of bubble growth, considering the extreme wetting scenarios of hydrophilicity and superhydrophobicity.

The images shown in the sequences b) and d) result from the post-processing of the sequence of images shown in a) and c), respectively, so they are not simulations or schematic representations. The respective temporal evolution of the bubble diameter and of the bubble contact angles are quantitatively shown in Figs. 10-12.

As expected, the bubble growth time on the superhydrophobic surface is much larger than that on the hydrophilic. This can be easily confirmed by looking at the temporal evolution of the bubble growth in Fig. 10: in the time one single bubble grows for the superhydrophobic surface, nearly 10 bubbles have grown and detached from the hydrophilic. Hence, while the bubble diameter slowly grows on the superhydrophobic surface over more than 300ms, attaining values larger than 10mm, bubbles over the hydrophilic surface grow up to 2-2.5mm, within around 10-16ms. The abrupt decrease of the

bubble diameter corresponds to its detachment instant. The corresponding bubble departure instant for the superhydrophobic surface could not be captured in this data set, as the growth period is too long. Having a closer look to the evolution of the departure diameter one can compare the experimental data with several theoretical predictions, as shown in Fig. 11. Many of these predictions mainly solve the energy equation, considering transient thermal conduction. Plesset and Zwick [10] assume a uniformly superheated thermal boundary layer around a spherical bubble and predict the bubble to grow asymptotically, following $t^{1/2}$. Alternative approaches (e.g. [11]) consider a non-uniform temperature distribution around the bubble, but predict the same trend of the bubble growth. More recently, Kim et al. [13,35,36] refer a different trend, proportional to $t^{1/3}$. The bubble growth is argued to be slower due to the fact that the pressure difference between the bubble and the liquid is not constant during growth, as simplified by the previously mentioned authors, but instead the vapor pressure inside the bubble should decrease as the bubble grows, so its actual growth rate should be slower. Afterwards, bubble growth is considered to be thermally dominated and to follow a trend with $t^{1/5}$, independently from the working fluid [36-38]. However, these authors use a refrigerant and very well wetting fluid, with very low surface tension, which may contribute to the deviations observed for the present data, with the hydrophilic surface. Hence, for our experimental data, the bubble radius has a fast increase within the first 1-3ms, which is approximately proportional to $t^{1/2}$ and only for later stages the bubble growth turns indeed proportional to $t^{1/5}$. Instead, the growth rate is quite slower for the bubble over the superhydrophobic surface (even slightly slower than $t^{1/5}$), probably due to the presence of the vapor blanket, which restricts the heat transfer to the bubble. This is in agreement with the low vaporization rate estimated in the beginning of this section, when analyzing the boiling curves and the average bubble diameters and emission frequencies.

Figure 9

Figure 10

Figure 11

Regarding the temporal evolution of the bubble contact angle, identified as illustrated in Figs. 9b) and 9d), on the hydrophilic surface (Fig. 12a), the bubble contact angle starts at a low value and then increases during bubble growth until the contact line starts receding. Afterwards, the angle further decreases until bubble detachment. Actually, the bubble contact angle starts with very low values (less than 50^{o}), which are not represented here, as the bubble at this period is yet too small to be accurately tracked and measured by the post-processing routine. The bubble contact angle increases up to around 135-140º during bubble growth up to its maximum diameter (for the first bubble represented in Fig. 10, this time

corresponds to nearly 8ms), decreasing afterwards at bubble detachment. This is still a macro-angle so it does not decrease to zero. Instead, a sudden discontinuity occurs at bubble detachment, which occurs at t≅15ms. Naturally that the macro-contact angle on the side of the surface, as defined by Phan et al. [3] has the opposite evolution, as it is mainly supplementary to the angle defined in the present study.

The temporal evolution described in these paragraphs is qualitatively in agreement with the process reported by [3], but the values obtained here are far from the quasi-static advancing and receding angles, shown in Table 2, so the approximation to these angles, as suggested by other authors, namely [3] does not seem to apply here.

On the other hand, given that for the superhydrophobic surface, the large bubble is formed already over a thin vapor film, it already appears with a shape that is indeed very close to that reported by [3] for hydrophobic surfaces, when the bubble is at its final stage and the radius keeps increasing while the contact angle remains nearly constant, during the entire slow growing process of the bubble, until it suddenly detaches from the surface (Fig. 12b). However, also in this case, the values of the macro or of the bubble contact angle do not seem to match to the advancing contact angle presented in Table 2.

Figure 12a

Figure 12b

It is worth mentioning that the oscillations between 70º and 75º come from the resolution of the measurement procedure itself which are dependent upon the number of useful border pixels to measure the angle. Hence, due to the shape of the bubble from the superhydrophobic surfaces, resolution is lower capturing angle changes above that threshold. To better infer on the stability of the actual bubble's growth process, the motion of the contact line is monitored during the time required for a single bubble to grow and detach from the surface in both hydrophilic and superhydrophobic cases, as represented in Fig. 13.

Hence, on the hydrophilic surface (Fig. 13a) the bubble has a stable contact line motion during the whole growth process, having one peak at the beginning of the bubble growth, which corresponds to the instant in which the bubble is visible for the first time. The velocity of the contact line slowly decreases then, until the maximum bubble size is reached at nearly 8ms, in agreement with the analysis of the bubble diameter and contact angle, performed in the previous paragraphs. Around this instant, the contact line velocity becomes close to zero. Afterwards it slowly starts to accelerate again during the receding motion, when buoyancy effects start to lift the bubble, pulling it away from the surface. Following the convention signs identified in Fig. 9, the receding motion is identified by the negative values of the velocity. The contact line does not decelerate until bubble detachment, which is identified by the sudden velocity increase back to zero.

Figure 13

Instead, for the bubble on the superhydrophobic surface, the contact line depicts an unstable motion, with many oscillations occurring stochastically throughout the growth process. The contact line follows almost like a wave movement along the growth process, which is also associated to the aforementioned instabilities in growth. Due to the large amount of data required to represent the entire process until bubble detachment, with the high temporal resolution used here, only half of the process is represented. However, the entire process was recorded and consistently presents the occurrence of these stochastic instabilities. Three main reasons can be pointed to explain this behaviour: the most likely is the "quasi-Leidenfrost" effect reported by [27], given that the vapour layer on top the surface, from which the bubble rises is much larger than the actual bubble, thus allowing it to go back and forth on top of this layer. In addition, the actual bubble size may also contribute to this instability, as the larger size of the bubble is mainly associated to the fact that buoyancy is balanced against the surface tension forces, maintaining the bubble close to the surface, which can induce instabilities. Finally, the actual slowness of the growth process may also allow for the local pressure variations to produce some effect on the bubble shape, which in turn would affect the size and position of the contact line.

3.3. Parameters quantifying the effect of wettability on bubble dynamics

Overall, the analysis performed up to now, describes the process of bubble growth and detachment which is in agreement with that reported in previous studies in the literature, namely by Phan et al. [3], when boiling occurs over hydrophilic surfaces. On the other hand, the bubble growth on the superhydrophobic surfaces is rather different, due to the formation of the stable vapour blanket, at very low superheating values (1-3K) which affects the bubble growth process as well as boiling curve.

From the quantitative point of view, there are some differences to point out in both hydrophilic and superhydrophobic cases, when compared to the literature. Hence, contrarily to the theory considered, for instance in [3], the contact line motion is significant, reaching values around zero only at maximum bubble diameter. Also, looking at the values of the bubble contact angle, which is mainly the supplementary of the macro-angle defined in Phan [3], it is not clear that any of these angles approach the receding and advancing angles, respectively as the bubble reaches its maximum diameter and afterwards when it detaches from the surface. Within this scope, one may perform a simple quantitative evaluation of the validity of using this macro-contact angle in the correlation proposed by Phan et al. [17] :

$$D_b = \left(6\sqrt{\frac{3}{2}}\right)^{1/3} \left(\frac{\rho_l}{\rho_v}\right)^{-1/2} \left(\frac{\rho_l}{\rho_v} - 1\right)^{1/3} (\tan\theta)^{-1/6} L_c \qquad (4)$$

in which $L_c = \sqrt{\frac{\sigma}{g(\rho_l - \rho_v)}}$ is the capillary length.

The results, depicted in Table 4, show a qualitatively correct trend of the bubble diameter to decrease with the macro-contact angle, in agreement with Phan et al. [3,17] but there is a significant disparity between the experimental values of the bubble diameter at detachment and those predicted by the correlation. It is worth mentioning that the experimental values obtained for the bubble departure diameter are in agreement with those reported in the literature (e.g. [21,22,39]).

Table 4

The number of cases that are available for comparison is very small for a conclusive analysis, since, despite nearly 40 cases were analyzed in the present work, the contact angles and the measured diameters are very similar, so a wider range of contact angles will be required for a proper evaluation. Nevertheless, the use of the macro-angle may still not be the correct one, but provides a correct trend. Regarding the approximation from the macro-contact angle as measured during bubble growth (the approach used in the present work) and the quasi-static angles, which is suggested in the literature, looking at the trend of the bubble diameter with these angles, as depicted in Fig. 14, they follow exactly the same trend, but the quantitative values are quite different. Consequently, any satisfactory result comes out from eq. (4) when using such approximation. Hence, this approximation is practical for a qualitative evaluation, but should not be used for the estimation of the bubble departure diameter. Additional work is now required to describe the bubble growth on the superhydrophobic surface, given that the initial contact angle is much higher than the 90º, which is the limit for several correlations reported in the literature, including the one given in eq. (4). In this case, the bubble growth over the vapour film must be already considered since, although this is not the starting point of the boiling process, it represents the actual working conditions when using this kind of surfaces.

Figure 14

3. Final remarks

The present study addresses the description of the heat transfer and bubble dynamics processes occurring at the boiling of water over surfaces with extreme wetting regimes, namely hydrophilicity and superhydrophobicity, which are mainly obtained by modifying the surface chemistry. Under these conditions and for the range studied here the effect of the extreme wetting regimes was dominant. Hence, the influence of surface topography was not addressed here.

In agreement with the literature, the onset of boiling occurs at much lower surface superheat for the superhydrophobic surfaces. However, a quite atypical boiling curve is obtained: the heat flux increases almost linearly with the superheat, until reaching a maximum value, after which it does not further increase. This trend is in agreement with the so-called “quasi-Leidenfrost” regime, recently reported in the literature. In the observed phenomena a film vapor is almost immediately formed at 1K of superheating, covering the entire surface, thus the heat transfer is reduced just after the onset of boiling. This evolution of the boiling curve is also in agreement with correlations for film boiling, which take into account the presence of a stable vapor layer, as observed here.

Bubble dynamics is useful to understand such atypical boiling curves, so a detailed analysis of bubble dynamics is presented, focusing on the temporal evolution of the bubble growth diameter together with bubble contact angle. Furthermore, contact line velocity profiles obtained for the bubbles growing on the superhydrophobic surfaces was shown to be highly unstable, contrasting to the stable growing process depicted on the hydrophilic surfaces. This instability is attributed to the large bubble size, to the vapour layer resulting

from the “quasi-Leidenfrost” phenomenon and to the slowness of the growth process, which allows the bubble to be affected by pressure variations, occurring within minutes.

Bubble dynamics analysis show that using the macro-contact angle i.e. the macroscopic contact angle supplemental to the bubble angle in correlations to predict the bubble departure diameter provides an accurate trend, although non-negligible disparities are still obtained when comparing the experimental data with the predicted values. Also, approximating the macro-contact angles measured during bubble growth to the quasi-static angles which can be obtained a priori during surface characterization is practical for a qualitative evaluation, but should not be used for the estimation of the bubble departure diameter.

Additional work is required to describe the bubble growth on the superhydrophobic surface, given that the initial contact angle is much higher than the 90º, which is the limit for the correlations tested. The effect of the vapour film formed on these surfaces at very low superheats must be considered since although this is not the starting point of the boiling process, it represents the actual working conditions of bubble growth and heat transfer, when using this kind of surfaces.

Acknowledgements

The authors are grateful to Fundação para a Ciência e a Tecnologia (FCT) for partially financing the research under the framework of the project RECI/EMS-SIS/0147/2012 and for supporting T. Valente with a research fellowship. The authors also acknowledge FCT for financing the Post-Doc fellowship of A.S. Moita (SFRH/BPD/109260/2015) and the PhD scholarship (SFRH/BD/88102/2012) of E. Teodori.

Finally, the authors acknowledge also the European Cooperation in Science and Technology — MPNS COST Action MP1106 “Smart and green interfaces — from single bubbles and drops to industrial, environmental and biomedical applications” led by Prof. T. Karapantsios.

Bibliography

[1] G. Klein, J. Westwater, Heat transfer from multiple spines to boiling liquids, *AIChE J.* 17(1971) 1050-1056.

[2] Y. Takata, S. Hidaka, L. Hu, Boiling feature on a super water-repellent surface, *Heat Transf. Eng.* 27(2006)25-30.

[3] H. Phan, N. Caney, P. Marty, S. Colasson,
Surface wettability control by nanocoating: the effects on pool boiling heat transfer and nucleati on mechanisms, *Int. J. Heat Mass Transf.* 52(2009) 5459-5471.

[4] B. Bourdon, R. Rioboo, M. Marengo, E. Gosselin, J. de Coninck, Influence of the wettability on the boiling onset, *Langmuir* 28(2012) 1618-1624.

[5] B. Bourdon, P. Di Marco, R. Rioboo, M. Marengo, J. de Coninck, Enhancing the onset of pool boiling by wettability modification and nanometrically smooth surfaces, *Int. Comm. Heat Mass Transf.* 45(2013) 11-15.

[6] B. He, A. Patankar, J. Lee, Multiple equilibrium droplet shapes and design criterions for rough hydrophobic surfaces, *Langmuir* 19(2003) 4999-5003.

[7] B. Bhushan, Y. Jung, Natural and biomimetic artificial surfaces for superhidrophobicity, self cleaning, low adhesion and drag reduction, *Progr. Mat. Sci.* 56(2011) 1-108.

[8] C. Antonini, A. Amirfazli, M. Marengo, Drop impact and wettability:from hydrophilic to superhydrophobic surfaces, *Phys. Fluids* 24(2012) 102104.

[9] S. Bankoff, Ebullition from solid surfaces in the absence of a pre-existing gaseous phase,*Trans. Am. Mech. Eng.* 79(1957) 735-740.

[10] M. Z. S. Plesset, The growth of vapour bubbles in superheated liquids, *J. Appl. Phys.* 25(1954) 493-500.

[11] B. Mikic, W. Rohsenow, P. Griffith, On bubble growth rates, *Int. J. Heat and Mass Transf.* 13(1970) 657-666.

[12] P. Cheng, X. Quan, S. Gong, F. Hong, Recent studies on surface roughness and wettability effects in pool boiling, *Proc. 14 th Int. Heat Transf. Conf. IHTC, Kyoto, Japan, 10-15 August,* 2014.

[13] J. Kim, H. Lee, B. Oh, M. Kim, Effects of bubble shape assumption on single bubble growth behaviour in nucleate pool boiling, *J. Flow Visualization Image Processes,* 11(2004) 73-87.

[14] W. Fritz, Maximum Volume of vapour bubbles, *Phys.Z* 36(1935) 379-388, 1935.

[15] M. Matkovic, B. Koncar, Bubble departure diameter prediction uncertainty, *Science and Tech. Nuclear Inst.,* vol. 2012, 2012.

[16] J. Mitrovic, Formation of a liquid jet after detachment of a vapour bubble," *Int. J. Heat and Mass Transf.,* 40(1997) 4309-4317.

[17] H. Phan, N. Caney, P. Marty, S. Colasson and J. Gavillet, "A model to predict the effect of contact angle on the bubble departure diameter during heterogenous boiling," *Int. Comm. Heat Mass Transf.,* vol. 37, pp. 964-969, 2010.

[18] A. Mukherjee and S. Kandlikar, "Numerical study of single bubbles during nucleate pool boiling," *ASME J. Heat Transfer,* vol. 126, pp. 1023-1039, 2007.

[19] Y. Takata, S. Hidaka, M. Kohno,
Effect of surface wettability on pool boiling: enhancement by hydrophobic coating, *Int. J. Air-Conditioning and Refrigeration,* vol. 20, 2012.

[20] A. Betz, J. Jenkins, C. Kim, D. Attinger, Boiling heat transfer on superhydrophobic, superhydrophilic, and superbiphilic surfaces, *Int. J. Heat Mass Transf.* 57(2013) 733-741, 2013.

[21] J. McHale, S. Garimella,
Bubble nucleation characteristics in pool boiling of a wetting liquid on smooth and rough surfac es, *Int. J. Multiphase Flow* 36(2010) 249-260, 2010.

[22] A. Moita, E. Teodori, Moreira and A.L.N., Influence of surface topography in the boiling mechanisms, *Int. J. Heat Fluid Flow* 52(2015) 50-63.

[23] J. Kim, Review of nucleate pool boiling bubble heat transfer mechanisms, *Int. J. Multiphase Flow* 35(2009) 1067-1076.

[24] A.L.N. Moreira, Multiscale interfacial phenomena and heat transfer enhancement, *Proc. 14 th Int. Heat Transf. Conf. IHTC, Kyoto, Japan, 10-15 August,* 2014.

[25] E. Teodori, A. S. Moita, A. L. N. Moreira, Empirical and modelling based correlations for pool boiling over micro-structured surfaces, *J. Int. Phen. Heat Transf.* 2(2014) 273-292.

[26] M. Kato , A. Tanaka, M. Sasagawa, H. Adachi (2008) Durable automotive windshield coating and the use thereof US 8043421 B2, Patent US8043421 B2.

[27] I. Malavasi, B. Bourdon, P. Di Marco, J. de Conink, M. Marengo, Appearance of a low superheat “quasi-Leidenfrost” regime for boiling on superhydrophobic surfaces, *Int. Comm. Heat Mass Transf.* 63(2015) 1-7.

[28] P. Cheng, Automation of aisymmetric drop shape analysis using digital image processing, *PhD Thesis, University of Toronto,* 1990.

[29] R. Abernethy, R. Benedict, R. Dowdell, ASME measurements uncertainty, *J. Fluids Eng.* 107(1985) 161-164.

[30] P. Berenson, Film-Boiling Heat Transfer From a Horizontal Surface, *J. Heat Transf.* 83(1961) 351-356.

[31] P. Berenson, Experiments on pool-boiling heat transfer," *Int. J. Heat and Mass Transfer,* vol. 5, pp. 985-999, 1962.

[32] V. Dhir, Mechanistic prediction of nucleate boiling heat transfer – achievable or a hopeless task, *J. Heat Transf.* 128(2006).

[33] N. Zuber, Nucleate boiling: the region of isolated bubbles and the similarity with natural convection, *Int. J. Heat Mass Transf.,* 6(1963) 53-78.

[34] M. Jakob, W. Fritz, Versuche uber den Verdampfungsvorgang, *Forschungsgebiete des Ingenieurwesens* 2(1931) 435-447.

[35] J. Kim, H. Lee, B. Oh, M. Kim, Study of the initial growth of single bubble at saturated nucleate boiling, *5th Int. Conf. Multiphase Flow - ICMF 2004, Yokohama, Japan, 30 May - 4 June,* 2004.

[36] J. Kim, B. Oh, M. Kim, Experimental study of pool boiling temperature effects on nucleate pool boiling, *Int J. Multiphase Flow* 32(2006) 208-231.

[37] H. Lee, B. Oh, S. Bae, M. Kim, Single bubble growth in saturated pool boiling on a constant wall temperature surface, *Int. J. Multiphase Flow* 29(2003) 1857-1874.

[38] H. Lee, B. Oh, S. Bae, K. M.H., J. Lee, I. Song, Partial nucleate boilingon the microscale heater maintaining constant wall temperature, *J. Nucl. Sci. Techn.,* 40(2003) 768-774.

[39] C. Gerardi, J. Buongiorno, L.-w. Hu, T. McKrell, Study of bubble growth in water pool boiling through synchronized infrared thermometry and high-speed video, *Int. J. Heat Mass Transf.* 53(2010) 4185-4192.

Tables:

Table 1
Thermo-physical properties of water, taken at saturation at 1.013 x 10^5 Pa.

Property	**Value**
Saturation temperature T_{sat} (°C)	100
Liquid densivty ρ_l (kg/m^3)	957.8
Vapor density ρ_v (kg/m^3)	0.5956
Liquid ynamic viscosity μ_l (mN m/s^2)	0.279
Specific heat c_{pl} (J/kgK)	4217
Thermal conductivity k_l (W/mK)	0,68
Latent heat of evaporation h_{fg} (kJ/kg)	2257
Liquid surface tension σ_{lv} (N/m)x10^{-3}	58

Table 2
Surface characteristics

Category	Surface material	R_a (µm)	R_z (µm)	θ_{adv} (°)	θ_{rec} (°)	Hysteresis (°)
RAW	Stainless steel	0.06	0.09	85±1	<20	>10
ROUGH	Stainless steel	1.20	1.58	90±6	<20	>10
RAW SHS	Stainless steel coated with *Glaco*	0.06	0.09	166±1	164	2
ROUGH SHS	Stainless steel coated with *Glaco*	1.20	1.58	166±1	164	2

Table 3
Uncertainties in bubble dynamics parameters

Parameter	Max. error (%)	Evaluation method
Bubble diameter - D_b (mm)	9.1	$$\frac{\Delta D_B}{D_B} = \sqrt{\left(\frac{\Delta C_f}{C_f}\right)^2 + \left(\frac{2e_{db}}{D_B.C_f}\right)^2}$$ C_f is the calibration factor. Given that this is subjected to a random error depending on the positioning of the pixel ruler on the image, an uncertainty of ±5% is estimated for the worst case scenario. e_{db} is the uncertainty associated to the definition of the boundary of the bubble which is evaluated to be 4pixels, also for the worse case (smaller bubbles).
Contact line velocity – v(mm/s)	8.2	$$\frac{\Delta v}{v} = \frac{\sqrt{\left(\frac{\Delta C_f}{C_f}\right)^2 + \left(\frac{2\ ev}{\Delta x.C_f}\right)^2}}{\Delta \boldsymbol{x}}$$ Here, Δx is the advancing or receding distance of the contact line between consecutive frames.

Table 4
Bubble departure diameter as a function of the bubble macro-contact angle: comparison between the experimental results obtained in the present study and those provided by the expression proposed by Phan et al. [17].

Macro-contact angle (Supplemental to the bubble angle) (^{o})	Predicted data (model Phan et al. [17]) (mm)	Experimental data (mm)	Relative deviation (%)
54	1.34	3.11	132.09
57	1.31	2.27	73.28

Figure(s)

Figures:

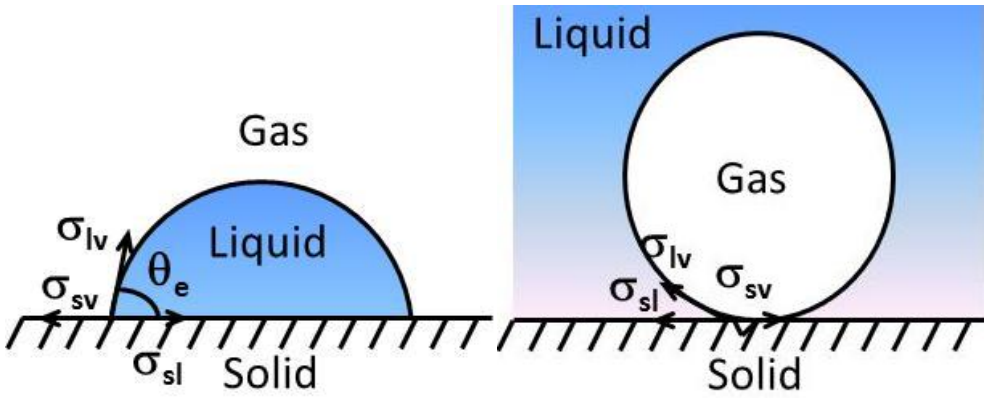

a) b)

Fig. 1. Balance of the interfacial tensions on: a) a droplet, b) a bubble over a hydrophilic surface).

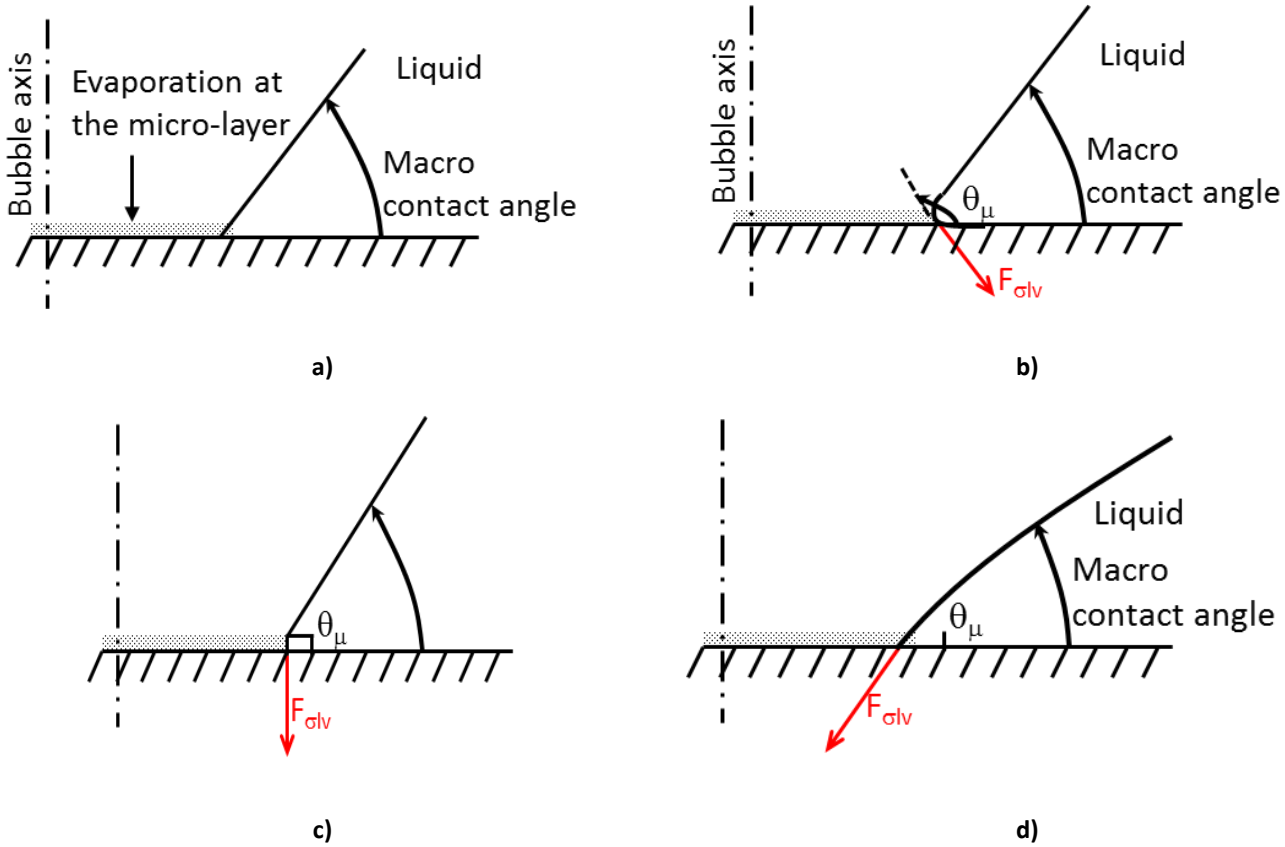

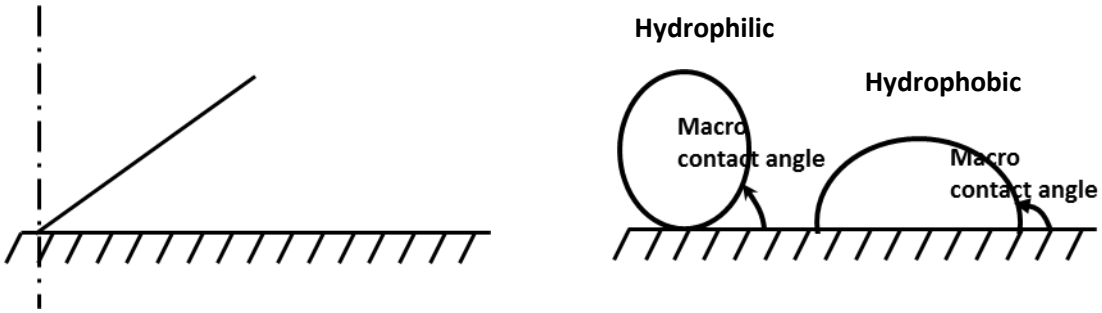

e) f)

Fig. 2. Bubble growth at a single nucleation site, following the theory of Phan et al. [3,17]: a) Evaporation leading to the distortion of the contact line, b) definition of the micro-contact angle θ_μ and of the actuating surface tension, c) definition of the micro-contact angle θ_μ and of the actuating surface tension at the limiting condition θ_μ=90º, d) contact line receding until bubble axis, e) bubble detachment, f) macro-contact angle for hydrophilic vs hydrophobic surfaces.

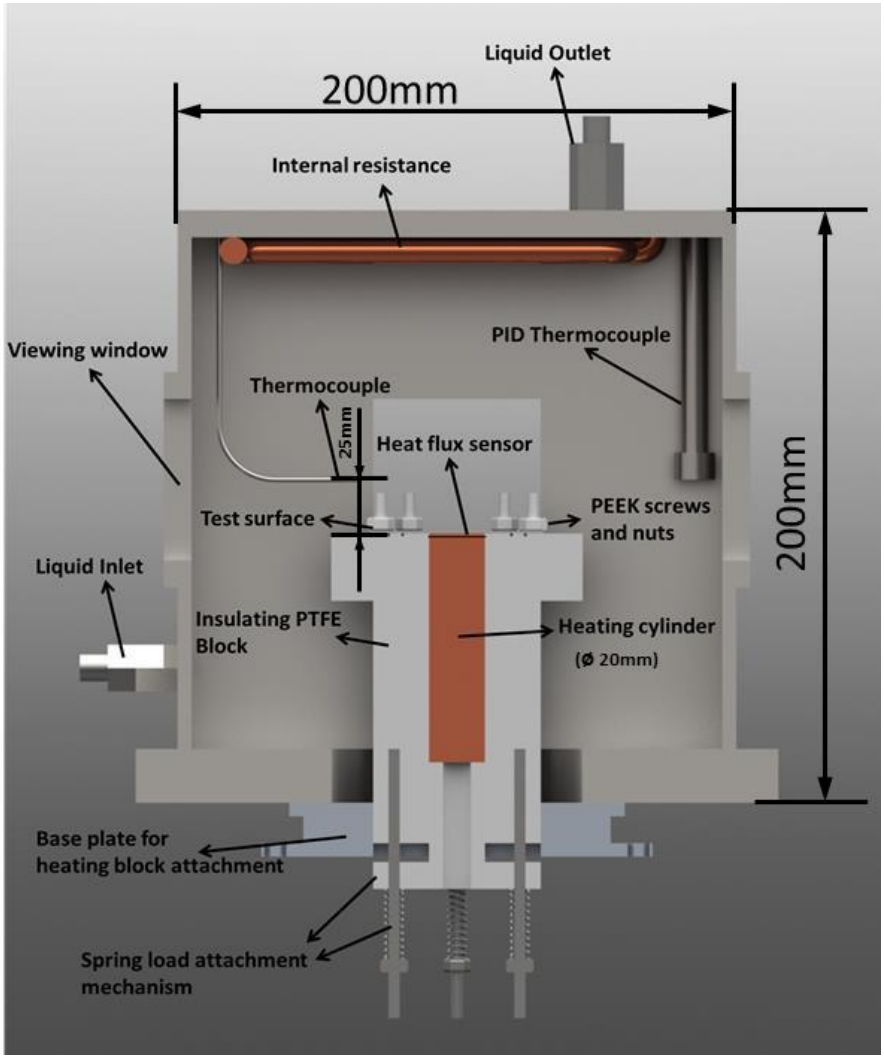

Fig. 3. Schematic representation of the boiling chamber.

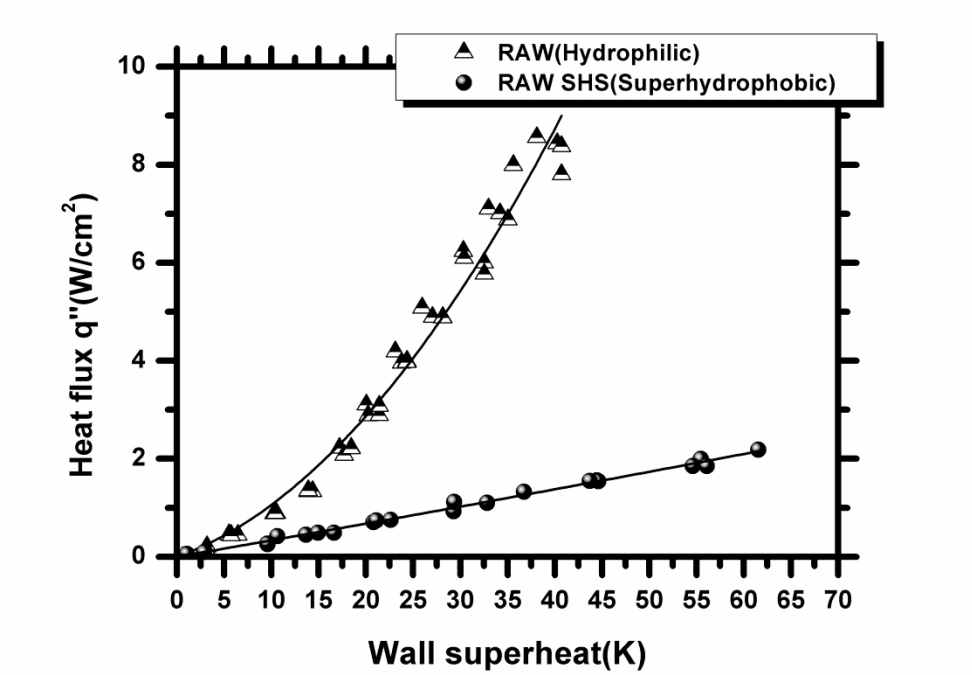

Fig. 4. Boiling curves obtained for water on hydrophilic and superhydrophobic stainless steel surfaces.

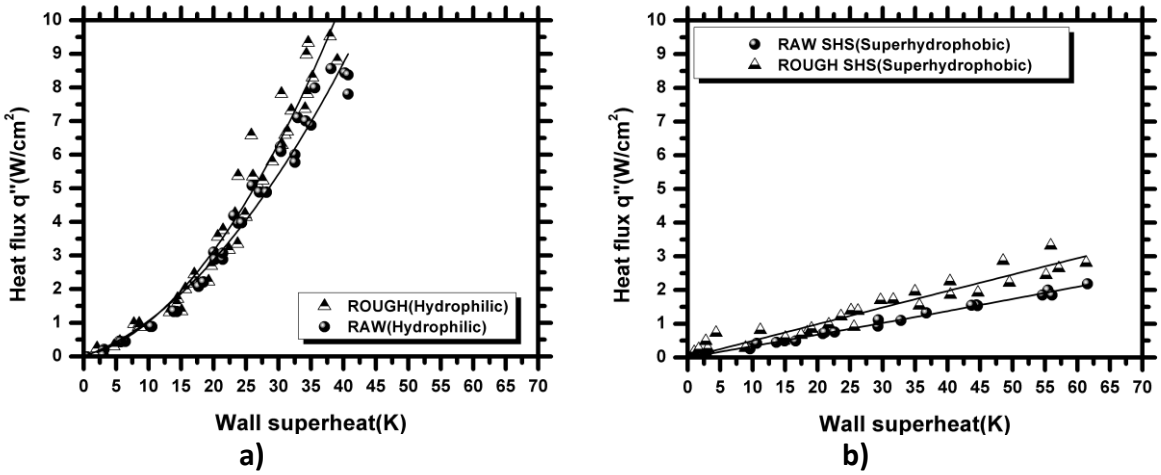

Fig. 5. Effect of surface topography (quantified by the parameters R_a and R_z depicted in Table 2 on the boiling curves of water on: a) hydrophilic surfaces, b) superhydrophobic surfaces.

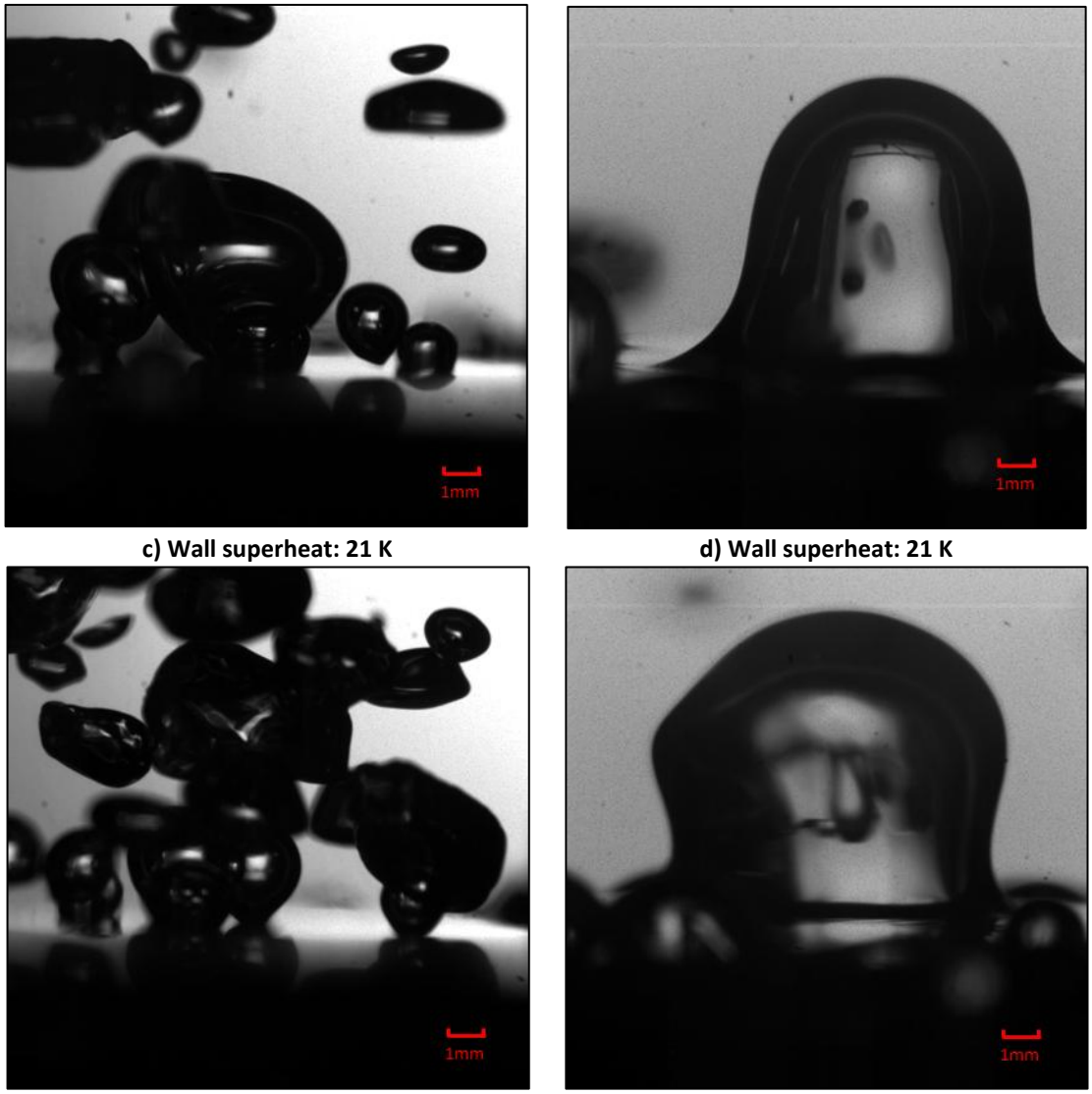

c) Wall superheat: 21 K **d) Wall superheat: 21 K**

e) Wall superheat: 40 K **f) Wall superheat: 44 K**

Hydrophilic surface **Superhydrophobic surface**

Fig. 6. High speed images of bubble dynamics for hydrophilic (left side) and superhydrophobic (right side) surfaces at various wall superheats. The complete videos are presented as supplemental material.

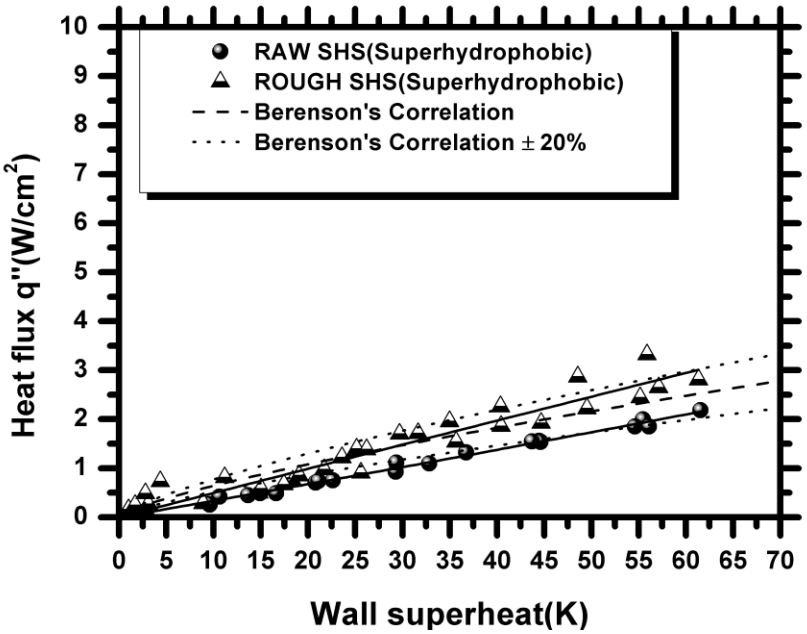

Fig. 7. Berenson's correlation as a qualitative description of the trend of the boiling curves obtained for the superhydrophobic surfaces.

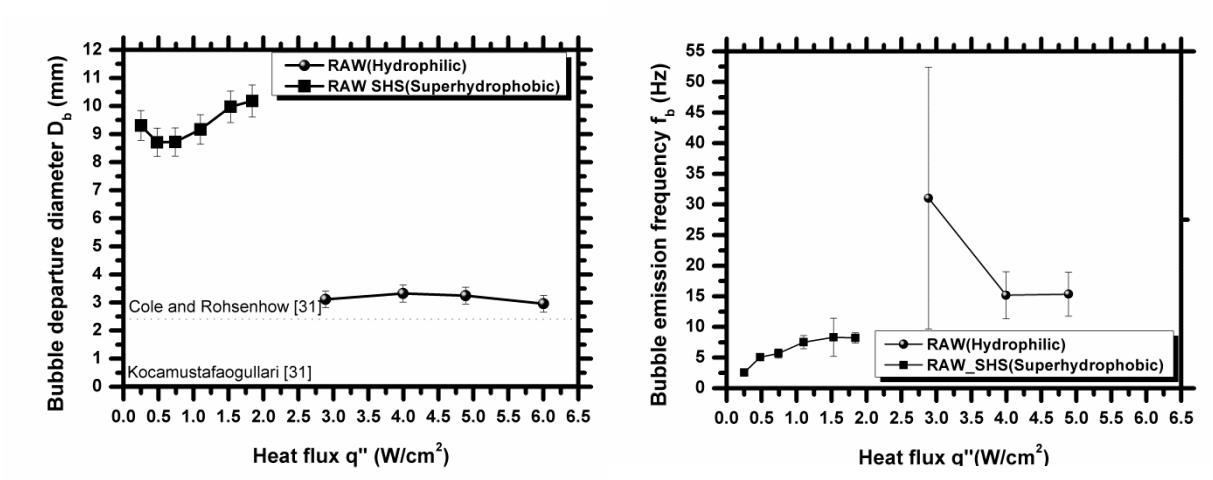

a) **b)**

Fig. 8. a) Average bubble departure diameters and b) emission frequencies, as a function of the imposed heat flux.

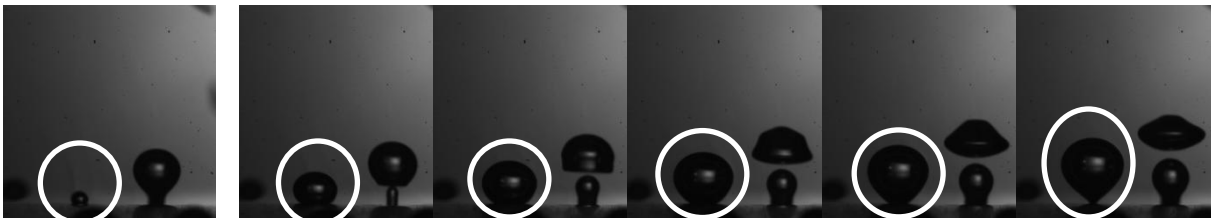

a)

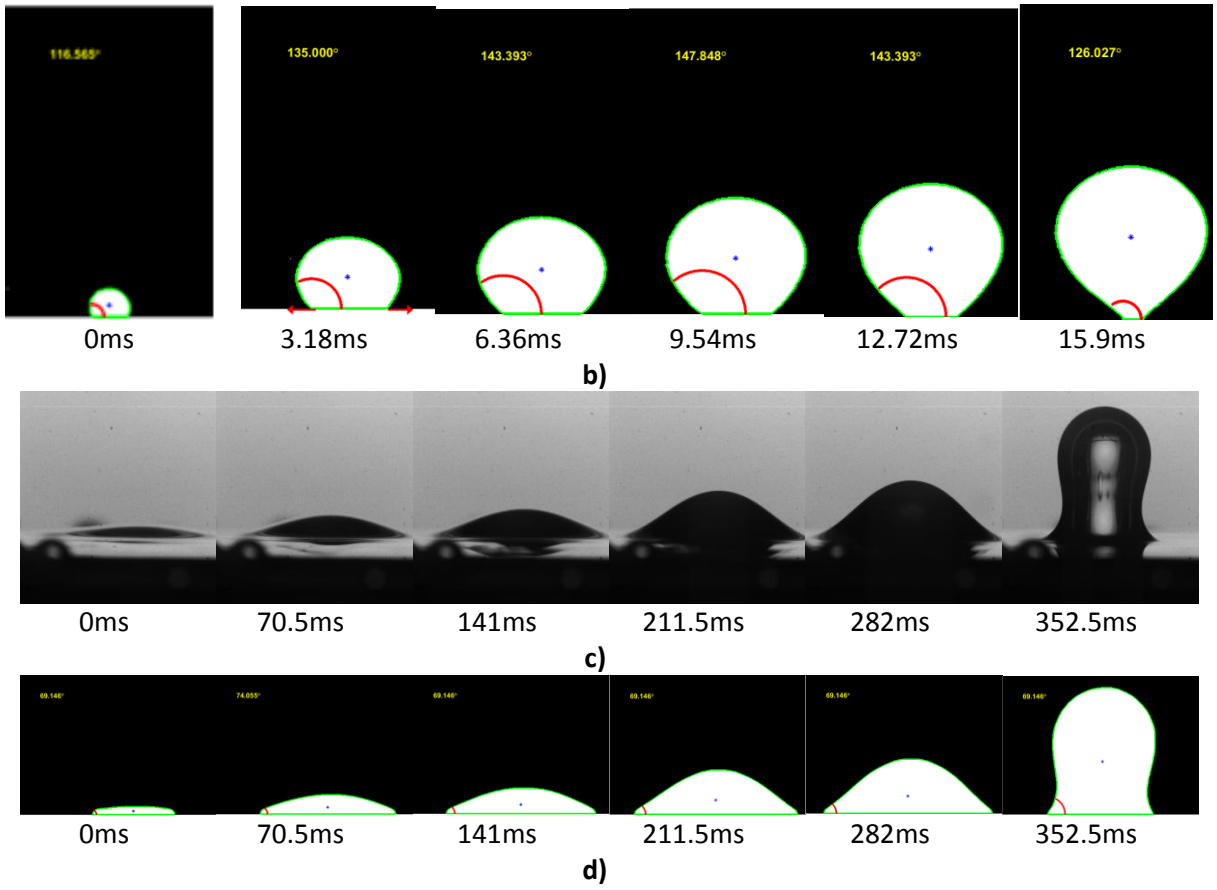

Fig. 9. Temporal evolution of the bubble growth and detachment on: a) a hydrophilic surface, b) a hydrophilic surface (post-processed images), c) a superhydrophobic surface, d) a superhydrophobic surface (post-processed images). The white circle identifies the bubble that is being measured on the hydrophilic surface. The lines in red in Fig 9b (3.18ms) schematically represent the sign convention used to compute the velocity of the contact line, as discussed later: advancing motion corresponds to positive velocity values, while negative values are associated to the receding motion.

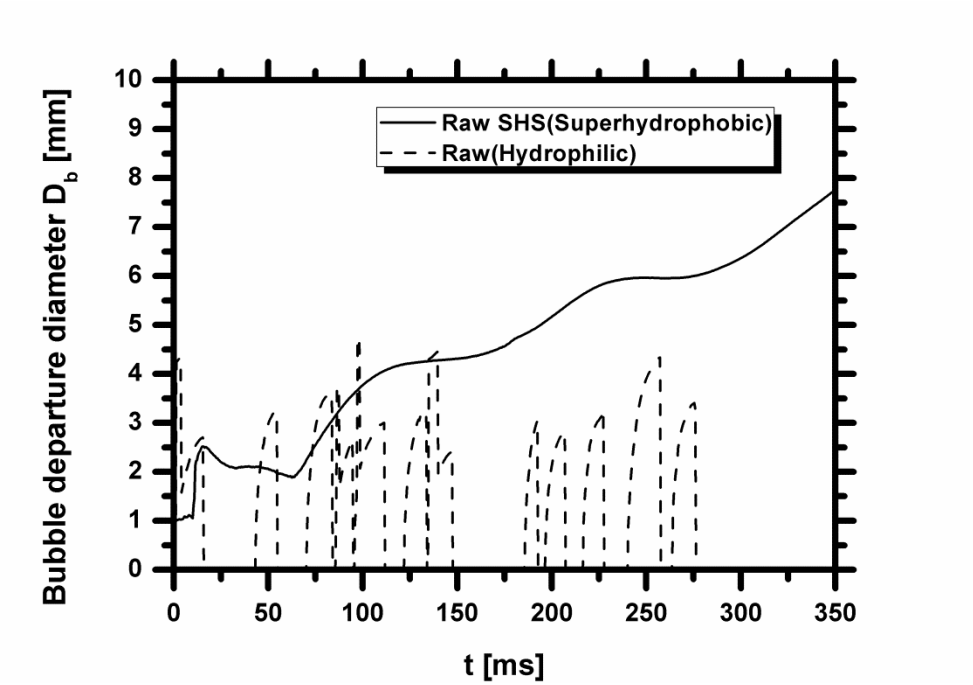

Fig. 10. Comparison between the bubble growth on a hydrophilic and a superhydrophobic surfaces at ≈ 10K of wall superheat.

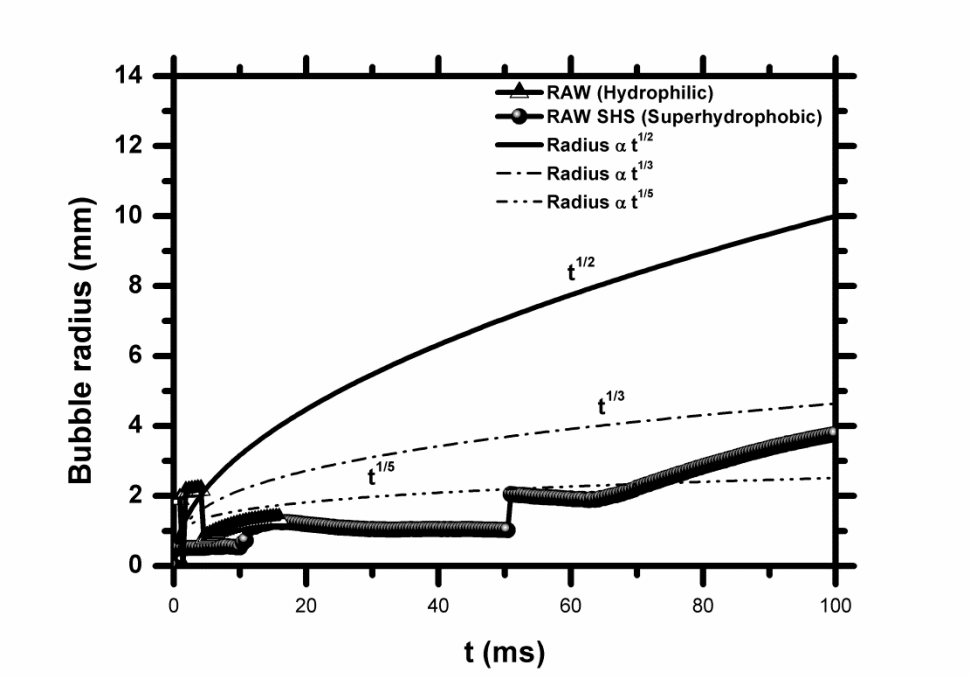

Fig. 11. Bubble growth on a hydrophilic and superhydrophobic surface at ≈ 10K of wall superheat: comparison with the theoretically predicted trends.

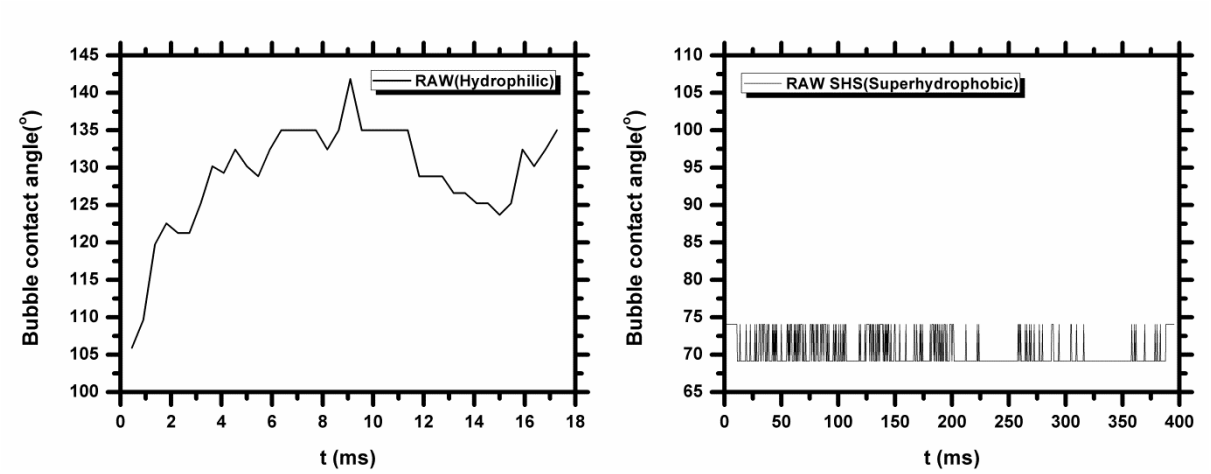

Fig. 12. Temporal evolution of the bubble contact angle during the growth and detachment of a single bubble on: a) a hydrophilic surface, b) a superhydrophobic surface.

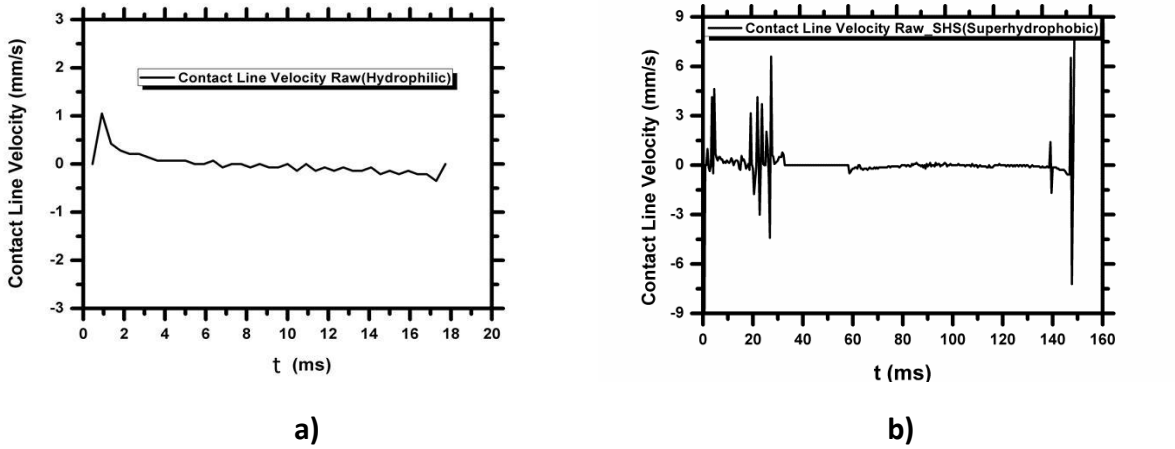

Fig. 13. Contact Line Velocity evolution for: a) a hydrophilic surface; b) a superhydrophobic surface.

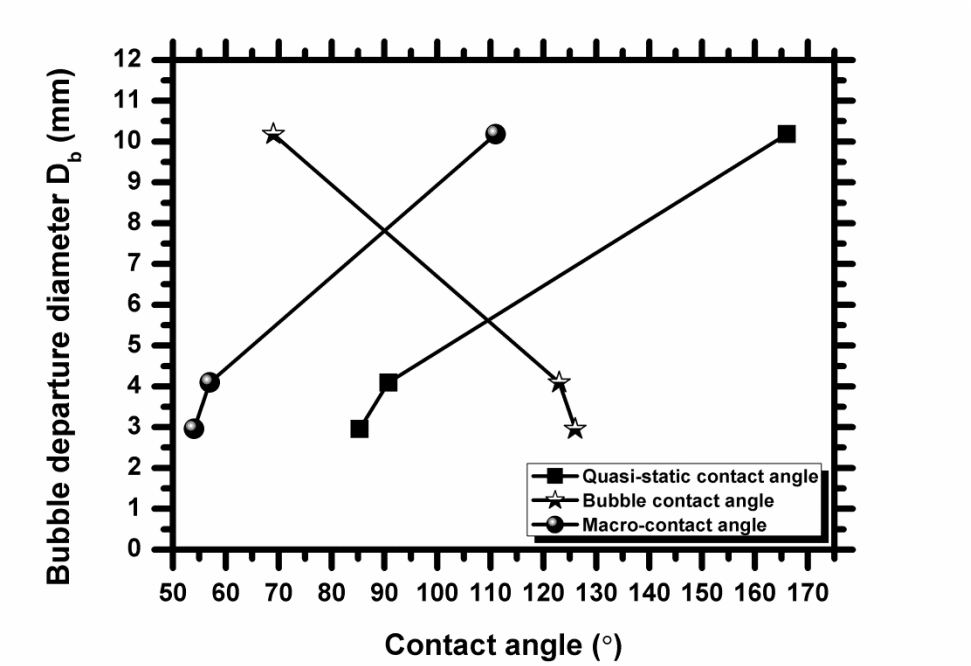

Fig. 14. Average bubble departure diameter as a function of the bubble contact angle, macro- contact angle and quasi-static angle.